Available online at www.sciencedirect.com
SCIENCE DIRECT
Fusion Engineering and Design 81 (2006) 1451–1458
Fusion Engineering and Design
www.elsevier.com/locate/fusengdes

Numerical study of MHD effect on liquid metal free jet under complex magnetic fields

Xiao-Yong Luo *, Alice Ying, Mohamed Abdou

Mechanical and Aerospace Engineering Department, UCLA, Los Angeles, CA 90095, United States

Received 6 February 2005; received in revised form 8 August 2005; accepted 8 August 2005
Available online 18 January 2006

Abstract

In this paper, we present numerical studies of liquid metal free surface jet characteristic behavior under the influence of transverse fields and field gradients. The goal of the numerical simulation study is to evaluate the usefulness of a proposed numerical scheme for MHD analysis by comparing the numerical results with experimental observations. A 3D liquid metal MHD code based on an induced magnetic field formulation was developed and a penalty factor numerical method was introduced in order to force the local divergence-free condition of the magnetic field. The proposed numerical techniques give reasonable results as compared to experimental findings at a high Hartmann number.

Keywords: Free jet; MHD; Numerical; High Hartmann number

1. Introduction

In a fusion device, the issue of how to protect the bottom part of the reactor interior is a problem. One solution to this problem is to use a divertor that consists of a liquid metal jet. To understand how liquid metal flows in a fusion environment, the three-dimensional effects associated with MHD free jet flows have to be investigated.

Despite the great development of computer resources and numerical methods over the past few decades, papers on the numerical simulation of MHD problems are relatively scarce. 3D simulations of MHD incompressible flows are even rarer, obtaining a 3D liquid metal MHD free jet solution is difficult, particularly because the free surface is involved. The complexities come from the actual description of physical phenomena and accurate mathematical description for the three components of the induced magnetic field at the physical boundaries and interfaces, as well as proper handling of the numerical challenges encountered in mesh schemes. These facts could lead to an inaccurate solution. However, without using 3D formulations the numerical solutions may not capture the real essence of the problems, and produce misleading results.

* Corresponding author. Tel.: +1 310 794 4452; fax: +1 310 825 1715.
E-mail address: xyluo@ucla.edu (X.-Y. Luo).

0920-3796/$ – see front matter © 2005 Elsevier B.V. All rights reserved.
doi:10.1016/j.fusengdes.2005.08.056

Considering that at any given point in time the velocity field of the main hydrodynamic quantity can be directly interacting with the main electromagnetic one (the magnetic field) without any interference, it is possible to build an MHD module into an existing CFD code (FLOW-3D [1] in this case) which has a verified Navier–Stokes' solver for turbulent free surface flows. In the present model, the MHD Lorentz force caused by the induced current is derived from Ampere's law by solving the induced magnetic field equations. A conservative formulation similar to Salah [2] is applied, which leads to the introduction of a penalty factor to impose the local divergence-free condition of the magnetic fields.

The objectives of this research include: to help define a lithium flow surface for NSTX field conditions through numerical investigation of liquid metal free jet behavior under transverse and transverse field gradient magnetic field environments; to study MHD effects on liquid metal jets and to compare the characteristic development of jets with and without magnetic fields; to provide sufficient data to guide and benchmark experimental results [3].

2. Numerical simulation

2.1. Governing equations

Under the influence of an external magnetic field, an electrically conducting incompressible viscous Newtonian liquid metal fluid is governed by Navier–Stokes equations, with a term incorporating the Lorentz force. The dimensionless form of the equations are:

$$\nabla \cdot \vec{U} = 0 \tag{1}$$

$$\frac{\partial \vec{U}}{\partial t} + (\vec{U} \cdot \nabla)\vec{U} = -\nabla p + \frac{1}{Re}\nabla^2 \vec{U} + N(\vec{j} \times \vec{B}) + \frac{1}{Fr} \tag{2}$$

$$\nabla \times \vec{E} = -\frac{\partial \vec{B}}{\partial t} \tag{3}$$

$$\nabla \times \vec{B} = \vec{j} \tag{4}$$

$$\vec{j} = Re_{\mathrm{m}}[\vec{E} + \vec{U} \times \vec{B}] \tag{5}$$

And the conservation law of the electric current density

$$\nabla \cdot \vec{j} = 0 \tag{6}$$

$$\nabla \cdot \vec{B} = 0 \tag{7}$$

Here Re, Re_{m}, N and Fr are the Reynolds, magnetic Reynolds, Stuart numbers and Froude number respectively. $\vec{U}$ is the velocity, $\vec{B}$ the magnetic field, p the pressure, $\vec{j}$ the current density, and $\vec{E}$ is the electric field.

In this paper, to determine induced current $\vec{j}$ and magnetic field B, the induced magnetic field equation and the conservation for the magnetic field under the classical MHD assumptions [4,5] can be expressed as:

$$\frac{\partial \vec{B}}{\partial t} - \nabla \times (\vec{U} \times \vec{B}) - \nabla \times \left(\frac{1}{Re_{\mathrm{m}}} \nabla \times \vec{B} \right) = 0 \tag{8}$$

where magnetic field B includes both the applied B_0 and induced B' fields. It should be pointed out that the magnetic free-divergence constraint (7) is implicit in Eq. (8). Indeed, if the divergence of Eq. (8) is taken term by term, the following condition on the divergence of B is obtained:

$$\frac{\partial(\nabla \cdot \vec{B})}{\partial t} = 0 \tag{9}$$

Eq. (9) implies that the divergence of B remains constant over time and thus zero if it is initially null. Solving the induction equation (8) and the continuity equation (7) for the magnetic field would normally result in an over-specified system of equations. This problem can be overcome by applying the continuity equation into the induction equation, while deriving a diffusion–convection Helmholtz-like equation,

$$\frac{\partial \vec{B}}{\partial t} + (\vec{U} \cdot \nabla)\vec{B} = \frac{1}{Re_{\mathrm{m}}} \nabla^2 \vec{B} + (\vec{B} \cdot \nabla)\vec{U} \tag{10}$$

This reduces the MHD system of Eqs. (7) and (8) to Eq. (5) with the appropriate set of boundary conditions. It should be noted that circumventing the constraint in Eq. (7) by solving Eq. (10) results in a much simpler system to solve. However Eq. (10) no longer states that the divergence of B remains constant over time. To solve this issue, a penalty factor is introduced to force the magnetic divergence toward zero based on the technique discussed in Refs. [2,5]. The technique calls for an addition of the gradient of a scalar variable q to Eq.

(10), which results in the following equation:

$$\frac{\partial \vec{B}}{\partial t} + (\vec{U} \cdot \nabla)\vec{B} = \frac{1}{Re_{\mathrm{m}}}\nabla^2 \vec{B} + (\vec{B} \cdot \nabla)\vec{U} + \nabla q \quad (11)$$

where $q = 0$ on the boundary and can be viewed as a Lagrange multiplier used to enforce the divergence-free condition.

2.2. Boundary conditions

Due to its 3D nature, the mathematics formulation for induced magnetic boundary conditions at the interface can be very complex. At present we do not know the precise boundaries. However, we expect that the magnetic field attenuates and vanishes at some distance in the insulating void because of the lack of a source of field generation [2,7]. A separate study is performed to estimate the "null" distance for a given field strength at the very front by setting velocity equal to zero in Eq. (10), while satisfying the divergent of B equal to zero. The calculation indicates that this distance is relatively short (<1 cm) for the field strength encountered in the present study (<tenth of T). Thus, the boundary conditions at some extended void boundaries are written as:

$$\vec{B} = 0 \quad (12)$$

However, at the extended void boundary, to ensure that the boundary conditions (12) are correct, we add a thick insulating void as the second domain (which surrounds the flow domain) to allow for the induced magnetic field to fall to zero at its outside boundary.

The volume of fluid method (VOF) [6] is used to calculate domain involves free surfaces .The electric conductivity at any free surface calculation cell varies according to the fraction of the fluid existing in the cell. The electric conductivity is estimated as:

$$\sigma_{\mathrm{e}} = F^* \sigma_{\mathrm{f}} + (1 - F)^* \sigma_{\mathrm{v}} \quad (13)$$

where σ_{f} and σ_{v} are the electric conductivity of fluid and void, respectively, and F is a volume function. The electric conductivity for the fluid/solid boundary cell is estimated in the same manner as in Eq. (13). So the induced magnetic fields are assumed to be continuous across interface S.

3. Results and analysis

Numerical calculations were performed to simulate experimental runs that were conducted at the UCLA MTOR facility [3]. The computational domain includes a nozzle opening of 5 mm located at the beginning of X-axis. The boundary conditions of flow field are continuative (except at the inlet boundary). All physical properties are these of Gallium's. Simulations were performed for inlet velocities of 3 and 5 m/s in order to compare with the experimental results.

3.1. A case with an initial jet velocity of 3 m/s

In this case, the computational domain is 200 mm × 12 mm × 12 mm and the total meshes are 120 × 22 × 22. The initial condition is uniform flow of 3 m/s ejecting from the nozzle. The corresponding Reynolds number is 46,000 and the mean Hartmann number is about 164. The magnetic field measured form the MTOR field is correlated as:

$$(B_y)_0 = 3.7681X^3 - 1.0386X^2 + 0.1572X + 0.5977$$

where X is the coordinates along the toroidal direction. The maximum magnetic field along toroidal direction is about 1.12 T while the minimum is about 0.6 T.

Fig. 1 shows the 3D velocity contours of our simulation at $t = 0.2$ s with/without magnetic field. The red color represents highest velocity while the blue means lowest velocity in the filed. Similar to the experimental result, we can see that with the gradient magnetic field the liquid metal jet did not show any deflection. However, the velocity decreased slightly as compared with no magnetic field. The maximum drops only 0.31%, which means that the MHD effect is not significant at this velocity. The induced current density in three directions is about 1.4×10^5, 4.5×10^5 and 4.7×10^5 separately while the induced magnetic field has a magnitude of 10^{-5}.

Fig. 2 shows changes in the liquid metal jet's radius with/without magnetic field downstream. The solid points with lines are the numerical results while the empty points are the experimental results. When with the MHD effect, the results of experimental and numerical coincide with each other very well. When without the MHD effect, some points of the experimental results fit with the numerical results while some points display oscillation. The reasons for this difference are:

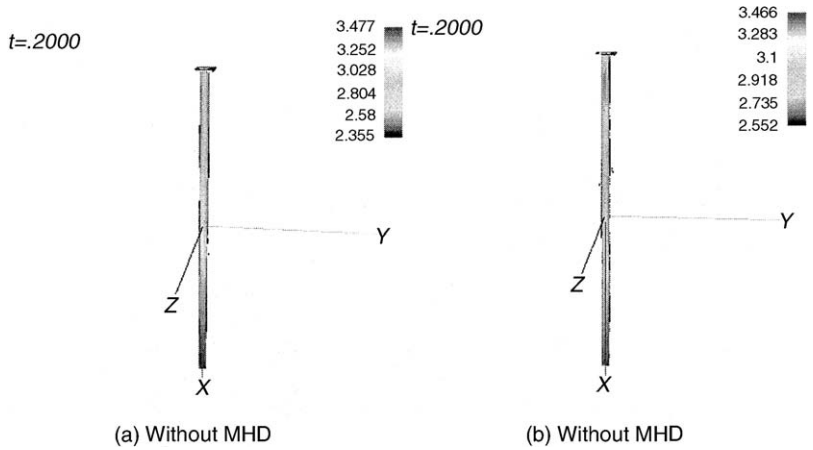

Fig. 1. 3D jet colored by x-velocity magnitude with/without field (initial velocity: 3 m/s).

(i) during the numerical simulation, we treat the initial condition of the free jet as ideal, which means we did not consider the effect of the nozzle configuration on the shape of the free jet. While in experiment, as we analysis before, we can actually see this effect: (ii) for the experiment, the initial instability plays a key role in the later free jet shape, such as the smoothness of the nozzle interior, the flow pump running condition and the vacum condition. While in the numerical simulation, we can think the initial jet is laminar without any disturbance and the boundary conditions are kept same during the computation.

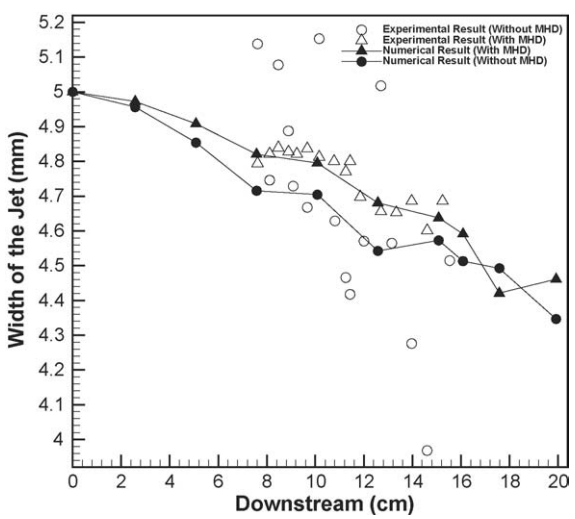

Fig. 2. Radius of the jet with/without magnetic field downstream (initial velocity: 3 m/s).

However, both results indicate that the MHD effect causes the jet radius to increase slightly as the jet proceeds downstream. The numerical results show the average radius of the jet increase is about 1.4%, and the area of the cross-section increase by about 2.9%. While the experimental results show that the width of the jet increases about 7%. Since the experimental results are only in toroidal direction and the cross-section of the jet is not change homogeneously, we cannot identify the change of the area of the free jet. Comparing these two results, we can see the numerical results are slightly smaller than the experimental results. This is because experimental results reflect only the width of the jet (a plane parallel to the flow direction). Cross-section variation along any other plan cannot be measured due to space limitations. In addition, the cross-section of the jet does not change uniformly in every direction, which implies that a single measurement cannot represent overall jet behavior. Due to the computational time limitation, we only get the numerical results for the first 20 cm, which is different from the experimental results.

Fig. 3 shows the induced current density J_y in the Y–Z cross-section downstream. The two positions here are $X = 2.5$ mm and $X = 194$ mm. The contours of J_x seem symmetric with respect to the Y-axis and Z-axis at the beginning part. Further downstream, the MHD effect breaks up the current loops first and then

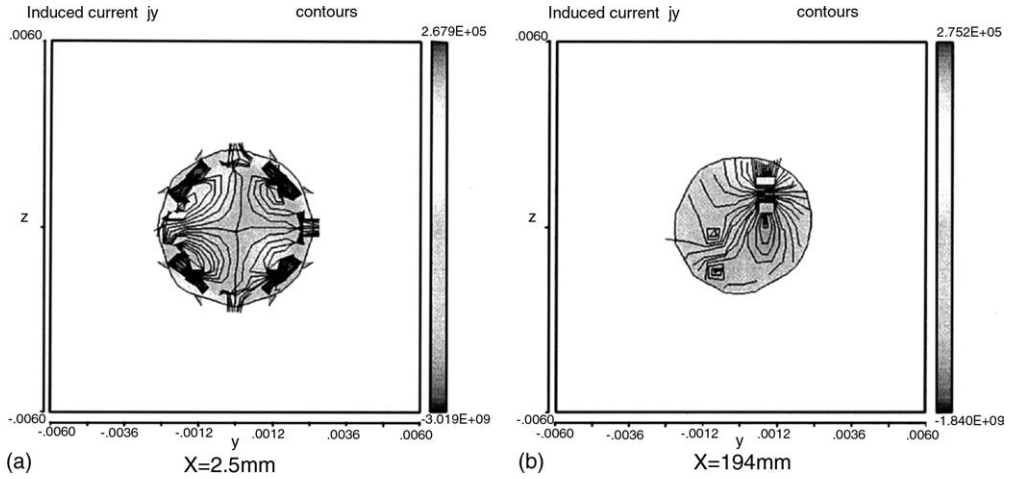

Fig. 3. Contours of induced current in *X*-direction (initial velocity: 3 m/s).

rearranges and finally recombines them into two large-loop structures that are almost symmetric around a 45° angle to the *Y*-axis.

Fig. 4 shows the induced magnetic field B_y in the *Y–Z* cross-section downstream. The two positions here are $X = 2.5$ mm and $X = 194$ mm. The MHD effects destroy the loop structures of induced magnetic field B_y. However, the symmetric feature of the contours still remains, where the axis also sits at a 45° angle to the *Y*-axis. This is mainly because the applied external magnetic field is along the *Y*-direction, which is much larger than the induced magnetic field that keeps the linearity of the Lorentz force.

3.2. A case with an initial jet velocity of 5 m/s

In this case, the computational domain is 200 mm × 10 mm × 8 mm and the total meshes are 180 × 22 × 22. The initial condition is a uniform flow of 5 m/s ejecting from the nozzle. The corresponding Reynolds number is 87,000 and the mean Hartmann number is about 164.

Fig. 5 shows the 3D velocity contours of our simulation at $t = 0.06$ s with/without magnetic field. Here we can see that with the gradient magnetic field, the liquid metal jet did not show any deflection. However the velocity decreased slightly as compared with that of

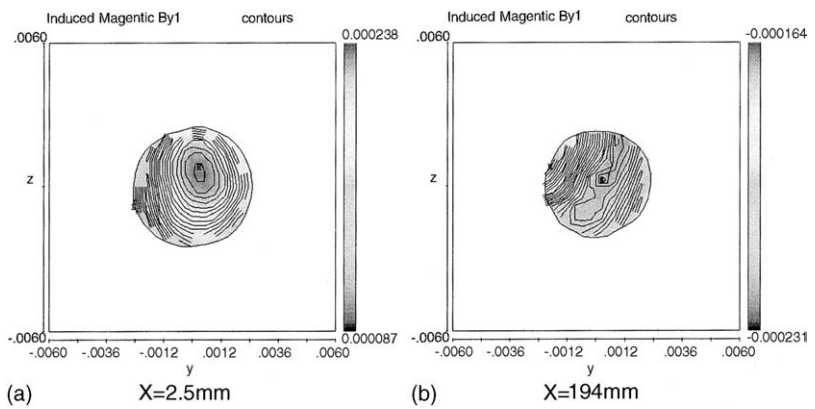

Fig. 4. Contours of induced magnetic field in *X*-direction (initial velocity: 3 m/s).

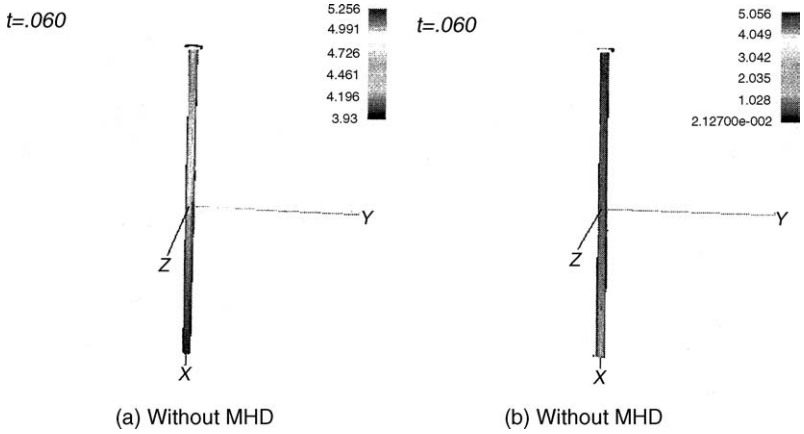

Fig. 5. 3D jet colored by x-velocity magnitude with/without field (initial velocity: 5 m/s).

no magnetic field. This result is verified by our experiment. The maximum is decreased by almost 3.8% with an MHD effect at this velocity that is almost 10 times as large as the conditions of 3 m/s. This means that the MHD effect is much more than a linear increase with the velocity. The nonlinear part dominates the MHD effect that is proved by our experiment, in which we increase the magnetic field by increasing the current.

Fig. 6 shows the liquid metal jet's radius change with/without magnetic field downstream. The solid points with lines are the numerical results while the empty points are the experimental results. When with the MHD effect, the results of experimental and numerical coincide with each other very well. When without the MHD effect, some points of the experimental results fit with the numerical results while some points display oscillation. The reasons are the same as the initial velocity equals to 3 m/s case. The numerical results indicate that the MHD effect causes the jet average radius to increase by about 5.1%, and the area of the cross-section to increases by about 10.5%. While the experimental results show that the width of the jet increases about 9%. Comparing these two results, we can see the numerical results are slightly smaller than the experimental results. The reason for this is same as we described in the previous case. The difference here from the last case is that the MHD effect is so strong that it can totally suppress the instability of the jet and the radius increase exponentially (which is same as the experimental results). The induced current density in three directions is about 2.7×10^5, 4.8×10^5 and 7.4×10^5 separately, which is much larger than the previous case.

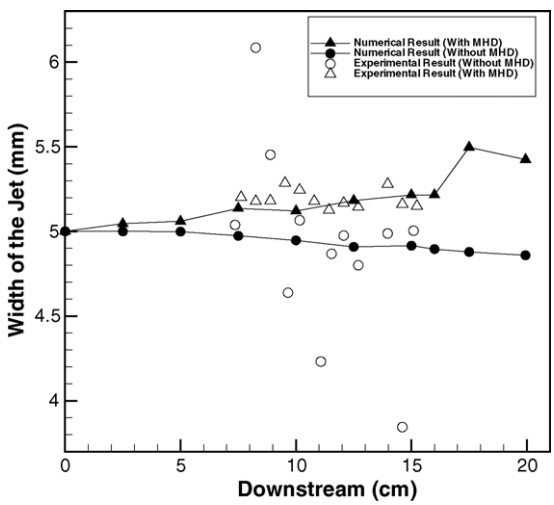

Fig. 6. Radius of the jet with/without magnetic field downstream (initial velocity: 5 m/s).

Fig. 7 shows the induced current density J_x contours in the Y–Z cross-section downstream. We chose six positions here so that we can see more details of the current loop structure changes. The contours of J_x are symmetric with respect to the Y-axis initially. Downstream, with velocity increasing such that the MHD effect increasing, the small loops first combine and form two large-loop structures. This status is not stable; the positive and negative parts mixed with each

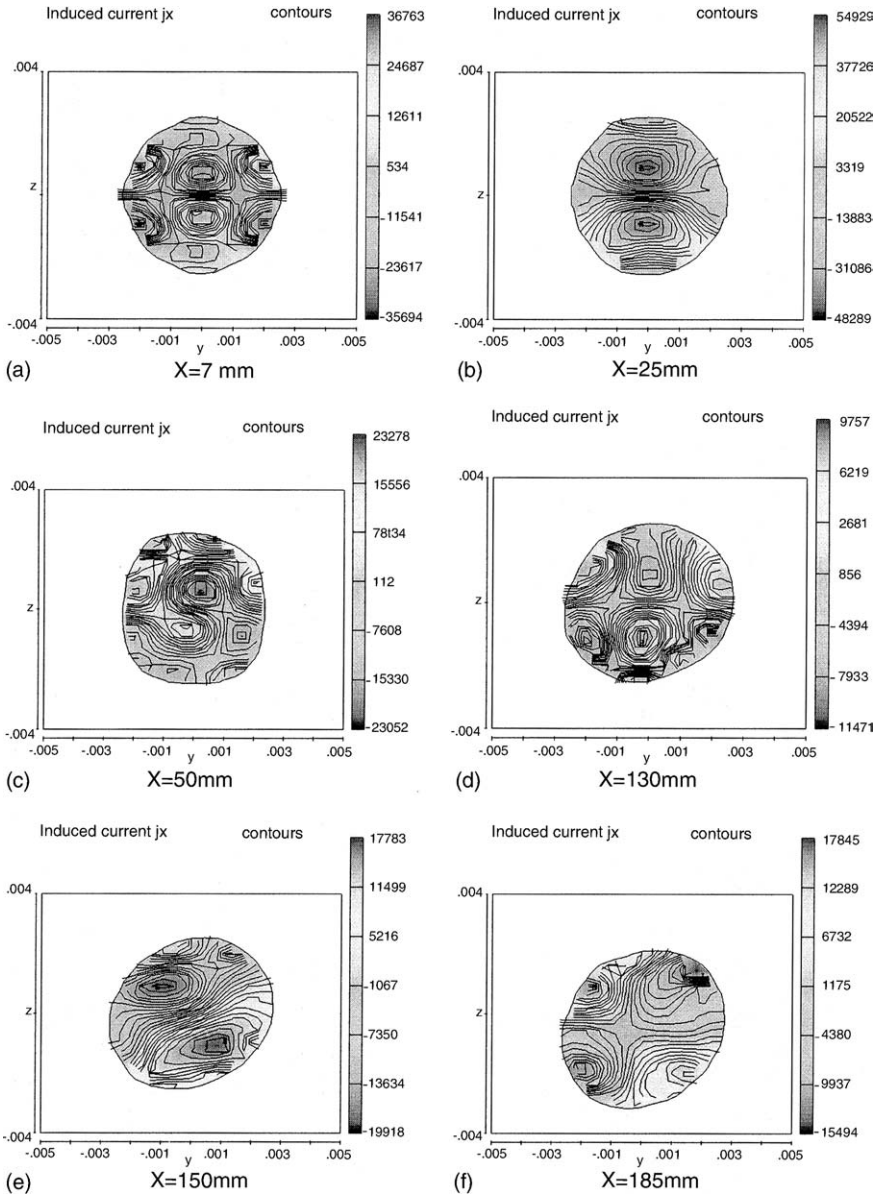

Fig. 7. Contours of induced current in *X*-direction downstream (initial velocity: 5 m/s).

other and at the same time break up into more small-loop structures. This mixing process causes the *Z*-axis symmetric to become slightly deflected. Further more, these small-loop structures combine again to form two large-loop structures that are symmetric around a 45° axis respective to the *Z*-axis. Finally, these loop structures break up into four small-loop structures again. This loop structure process is the same as we described in the experimental section. During this process, the cross-section shape was stretched along the 45° axis with respect to the *Z*-axis so that we can explain why little difference exists between the width of jet analysis in the experimental part and the radius of jet analysis in the numerical part.

4. Conclusion

This paper has presented a numerical study of liquid metal free surface jet characteristic behavior under the effect of transverse fields and field gradients. The numerical results verify the findings from the experimental results: liquid metal jet does not show any deflection under the gradient magnetic field; the width of the jet increases a little bit, although MHD effects are underestimated; the changes of the induced current form result in the turbulence suppressing. The numerical results show that with the MHD effect, the induced current $\vec{J}$ keeps the symmetric form while enduring the combing, rearranging, breaking process. This symmetric form means the MHD effect smoothes the chaotic motion inside the free liquid metal jet since the Lorentz force is mainly from the induced current and the original magnetic field. This turbulence suppressing mechanism can explain the eddy structures break down process in the experimental results. And the experimental results also verify this turbulence suppress phenomena by the MHD effect. However, from the numerical results we can see the induced magnetic field symmetric form has been destroyed by the MHD effect which will enhance the chaotic of the motion of the fluid.

Acknowledgements

The authors would like to thank N.B. Morley, M.-J. Ni for fruitful discussion. This work is supported by the U.S. Department of Energy under Grand No. DE-FG03-86ER52123.

References

[1] FLOW-3D User's Manual, Version 7.7, Flow Science Inc., 2000.
[2] N.B. Salah, A. Soulaimani, W.G. Habashi, A finite element method for magnetohydrodynamics, Comput. Meth. Appl. Mech. Eng. 190 (2001) 5867–5892.
[3] X.-Y. Luo, A. Ying, M. Abdou, Experimental and computational simulation of free jet characteristic under transverse field gradients, FST 44 (2003) 85–93.
[4] H. Branover, Magnetohydrodynamic Flow in Ducts, Isreal University Press, Jerusalem, 1978.
[5] L.D. Landau, E.M. Lifshitz, L.P. Pitaevskii, Electrodynamics of Continuous Media, Pergamon Press, Oxford, 1984.
[6] C.W. Hirt, B.D. Nichols, Volume of fluid methods for the dynamics of free boundaries, JCP 39 (1981) 201.
[7] S.S. Sazhin, M. Makhlouf, Solutions of magnetohydrodynamic problems based on a conventional computational fluid dynamics code, Int. J. Num. Meth. Fluid 21 (1995) 433–442.